Iranian Society of Acoustics and Vibration
The 15th ISAV2025 International Conference on Acoustics and Vibration
24-25 Dec 2025 Tehran- Iran

Analysis of Ultrasonic Guided Wave Transmission and Reception Angle for Selective Mode Excitation in Composite Pipes

Nima Dowlatabadi[1], MohammadHossein Soorgee [2*]

[1] MSc. Student, Faculty of Mechanical and Energy Engineering, Shahid Beheshti University, Tehran, Iran
[2] Assistant Professor, Faculty of Mechanical and Energy Engineering, Shahid Beheshti University, Tehran, Iran
** mh_soorgee@sbu.ac.ir*

Abstract

his study investigates the propagation characteristics of ultrasonic guided waves in glass-fiber-reinforced PMMA pipes using three distinct simulation models: a pure-PMMA wedge (Model 1), an infinite-element boundary wedge configuration (Model 2), and an epoxy-damped wedge (Model 3). Time-domain signals were analyzed to evaluate amplitude, peak characteristics, and energy distribution across different incident angles. Time-shifting and envelope analysis were employed to align signals and identify the first excited modes. The results reveal that the largest peaks and energy maxima occur at different angles depending on the model and time window considered. Models 2 and 3 consistently produced higher peak amplitudes compared to Model 1, demonstrating the influence of boundary condition implementation and damping on signal clarity and mode separation. Overall, incident angles of 40°, 45°, and 50° consistently yielded superior performance in terms of first-mode excitation, peak amplitude, and energy within the targeted time interval across all models. These findings indicate that optimal excitation for maximizing signal energy and first-mode detectability does not necessarily coincide with the angle of maximum total energy. The study highlights the importance of selecting incident angles based on initially excited modes for accurate guided-wave analysis and provides insights for improving nondestructive evaluation and structural health monitoring in composite piping systems.

Keywords: Ultrasonic guided waves; Composite pipes; Signal energy analysis; Mode excitation; Wedge Configuration

1. Introduction

Composite pipes have become among the most widely Utilized materials in modern industry [1]. The construction and infrastructure sector, including water, energy, and oil and gas industries, represent one of the largest consumers of composite materials [2]. This widespread adoption is driven by the exceptional combination of properties offered by composites, such as high specific strength and stiffness, low density, superior durability, excellent corrosion resistance, and long fatigue life [3]. These unique characteristics provide the mechanical engineer with design opportunities not possible with conventional monolithic materials [4]. Ensuring structural integrity throughout the service life of composite piping systems is critical, as failure in these materials are often internal and layered, and some defects may originate during manufacturing. Common issues include delamination, debonding of adhesive joints, resin voids, and inter-fiber cracks, which are typically undetectable through visual inspection or hydrostatic testing [5]. In this context, non-destructive evaluation (NDE) techniques have emerged as one of the most effective approaches for identifying and assessing damage, providing a reliable means to prevent failures and maintain operational safety [6].

Ultrasonic guided wave testing provides an advanced non-destructive approach for detecting defects in pipelines. Guided waves are mechanical waves that propagate along waveguide structures and are extensively employed in the non-destructive evaluation of plate- and pipe-like components [7]. Due to its ability to cover large areas from a single location, guided wave testing is especially advantageous for long-distance pipeline inspection in industrial applications [8]. Recent review studies indicate that guided wave ultrasonic testing remains an active research area, with challenges related to anisotropic materials, high attenuation in certain composites, and fluid-loading effects requiring focused investigation [9]. Multiple studies have demonstrated that Lamb-type ultrasonic guided waves are particularly sensitive to delamination in composite materials and can even enable the quantification of defect depth [10]. Delamination, voids, cracks, and resin-rich or resin-poor regions have been successfully identified in composite materials using ultrasonic techniques [11], [12]. However, most studies in this area have focused primarily on detecting matrix-reinforcement debonding and fatigue damage, highlighting the need for further investigation [13]. Yang et al. [14] modeled guided wave propagation in composite pipes using a semi-analytical finite element (SAFE) approach to accurately predict wave dispersion. Gresil et al. [15] investigated Guided wave propagation in hybrid carbon-glass fiber composite pipes through simulations and experiments, demonstrating effective damage detection and localization. Almeida et al. [13] applied ultrasonic methods to evaluate adhesive joint quality in glass-fiber-reinforced pipes, successfully detecting common defects such as lack of adhesion. Similarly, Soorgee and Jozani [16] used numerical simulations to investigate guided wave propagation in adhesive joints of composite pipes, confirming that guided waves can effectively identify joint defects.

In spite of all, this method also faces several challenges when applied to composite materials. One of the most significant issues is the inherent anisotropy of most composite pipes, which causes the wave propagation speed to be highly dependent on both the excitation direction and the propagation path, thereby increasing the likelihood of errors during inspection. In addition, the high damping characteristics of composite structures reduce the amplitude of received signals, making accurate defect detection more difficult. Unlike bulk ultrasonic waves, guided waves interact with the boundaries of the structure, exciting multiple modes whose propagation characteristics depend on the excitation frequency and the geometry of the component [17]. Wu et al. [18] addressed the challenge of analyzing multi-mode and dispersive guided wave signals in composites and proposed a novel Generalized Dispersive Mode Decomposition method, particularly effective for signals with overlapping time–frequency components. Abuassal et al. [19] provided foundational insights into ultrasonic guided waves, focusing on mode excitation, selection, and unidirectional signal generation and reception. Feng et al. [20] investigated the influence of composite layer thickness on guided wave propagation and damage localization, showing that thickness significantly affects wave characteristics, including the group velocities of A_0 and S_0 modes. Kazys et al. [21] studied higher-order Lamb modes (A_1 and S_1) in plastic and composite plates using non-contact techniques, demonstrating their potential for higher-resolution damage detection despite excitation challenges. Witt et al. [22] developed a phased-array method for selective excitation of guided wave modes in plate structures, enabling constant-phase-velocity mode excitation, particularly at high frequencies and large thickness–frequency products, with numerical simulations confirming its effectiveness.

For conducting a guided wave ultrasonic inspection, key criteria such as low dispersion, minimal attenuation, high signal energy, and the method of wave excitation and reception are typically considered. These factors facilitate simpler signal processing, extend inspection coverage, and assist in selecting modes that are optimal for the geometry of the component and the type of defect being investigated [23]. Due to dispersion, different frequency components of guided waves propagate at varying velocities. This phenomenon reduces temporal resolution and complicates the separation of modes in the received signal. Attenuation curves further indicate the frequency ranges in which a particular mode experiences minimal energy loss. Selecting modes that exhibit low attenuation at specific frequencies is crucial for achieving long-range coverage and maintaining a high signal-to-noise ratio. Each mode also exhibits a characteristic displacement pattern (radial–axial–circumferential), which determines its sensitivity to various defect types, such as longitudinal cracks, circumferential cracks, and delamination [23, 24]. Consequently, choosing the appropriate mode based on the geometry and material properties of the component is essential. Exciting the optimal mode—considering the structure, material, layering, fiber orientation, and angle of excitation—represents one of the most critical steps in the successful implementation of ultrasonic guided wave testing.

2. Materials and Model Description

A Glass Reinforced Vinyl ester (GRV) composite pipe was modeled in Abaqus CAE to study the propagation of guided ultrasonic waves and their interaction with the pipe's layered structure. The pipe had an outer diameter (OD) of 112 mm and a length of 170 mm. This length was selected to ensure that reflections from the pipe ends did not interfere with the main wave propagation region. The composite laminate was modeled with the stacking sequence [0, −63, 63, −63, 63, −63, 63], representing a symmetric configuration typical of GRV pipes. The layup consisted of one central felt layer with a thickness of 4 mm, surrounded by six Vinyl ester–glass layers, each 0.5 mm thick. This configuration resulted in a total wall thickness of 7 mm.

The pipe material was assumed to behave linearly elastic and orthotropic, with material properties derived from experimental data and literature [16]. Each composite layer was modeled as an individual part in Abaqus CAE, and the interfaces between the layers were assumed to be perfectly bonded to simulate a continuous laminate structure. The mesh was refined along the thickness direction to accurately capture the through-thickness stress and displacement variations associated with guided wave propagation. Two identical PMMA wedges were positioned on the outer upper surface of the pipe, separated by 30 mm along the axial direction and facing each other. The left wedge functioned as the transmitter, and the right wedge as the receiver. The wedge geometry was adapted according to the selected incident angle (ranging from 40° to 75°, in 5° increments), as shown schematically in *Figure 1*.

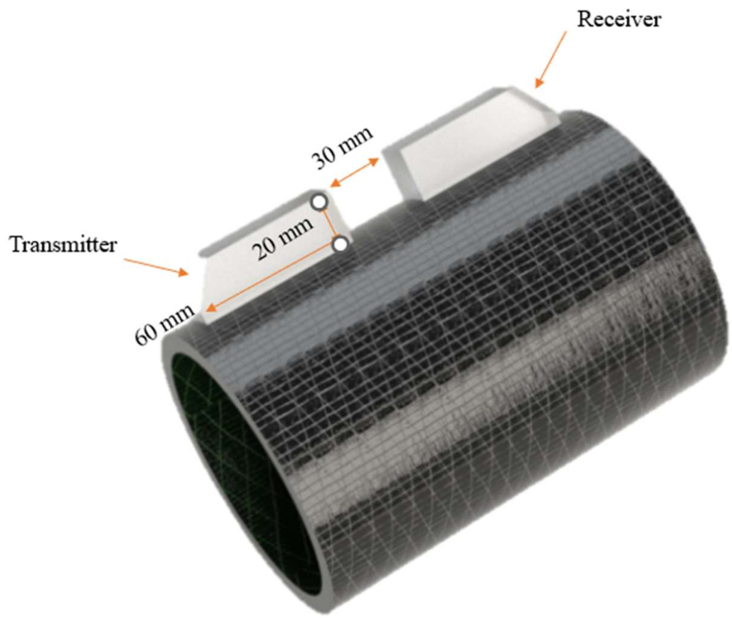

Figure 1) Schematic of the placement of PMMA wedges on the composite pipe at an incidence angle of 60°.

The elastic constants for the composite layers and the PMMA wedge material are summarized in *Table 1.*

Table 1) Mechanical properties of the composite layers and PMMA wedges

Material	E_1 (GPa)	E_2 (GPa)	E_3 (GPa)	ν_{12}	ν_{23}	ν_{13}	G_{12} (GPa)	G_{23} (GPa)	G_{13} (GPa)	ρ (kg/m^3)
Felt	14.0	14.0	5.0	0.3	0.1	0.1	6.0	4.0	4.0	1600
Vinyl ester–glass	38.0	3.0	3.0	0.0001	0.0001	0.0001	4.5	4.5	3.5	1800
PMMA (wedge)	3.0	–	–	0.37	–	–	–	–	–	1180

3. Methodology

3.1 Excitation and Signal Design

A 5-cycle tone burst with a frequency of 120 kHz was applied to the transmitting wedge. This frequency was chosen to ensure narrow-band frequency content and minimize modal overlap within the composite pipe. The receiving wedge recorded time-domain displacement signals, which were later analysed in both time and frequency domain, mode content, and Energy behaviour. The ultra-sonic wave is introduced into the wedge through pressure applied at its angled surface, allowing the wave to couple into the composite pipe.

3.2 Simulation Configurations

Finite element simulations were conducted under three different wedge configurations to assess the influence of boundary and damping conditions on wave propagation within the composite pipe.

3.2.1 Model 1 – Pure PMMA Wedge

In the first configuration, the wedge was modelled as a homogeneous PMMA block without any special boundary treatments. In this simplified model, a portion of the ultrasonic wave transmits into the pipe, while another portion reflects from the upper and lateral walls of the wedge. These reflections can re-enter the propagation path, leading to interference effects and increasing the complexity of the excited wave modes.

3.2.2 Model 2 – Wedge with Infinite Elements

In the second configuration, infinite elements were assigned to the upper and lateral boundaries of the wedge. These elements simulate an open boundary condition by absorbing outgoing waves, thereby preventing reflection back into the wedge. This setup effectively eliminates internal reflections and provides a more accurate representation of guided wave transmission into the composite pipe.

3.2.3 Model 3 – Wedge with Damping Epoxy

In the third configuration, a damping layer was added to the upper part of the PMMA wedge. Based on previous research, epoxy was chosen due to its strong attenuation characteristics. The damping layer absorbs and dissipates energy from waves reflecting within the wedge, reducing back-reflections. This configuration closely resembles practical experimental setups where damping materials are employed to minimize internal reflections and enhance measurement accuracy.

Figures 2 and 3 illustrate the wave propagation contours and pressure distribution on the wedges and the pipe at two different time instances. The displacements in both the pipe and wedges are magnified by a scale factor of 15,000 to clearly visualize the various wave modes over time.

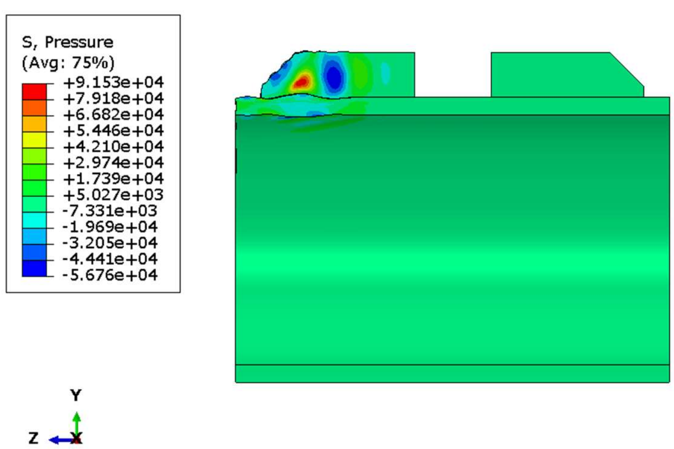

Figure 2) Pressure contour at increment 6667 and time 3.3337×10^{-5} s.

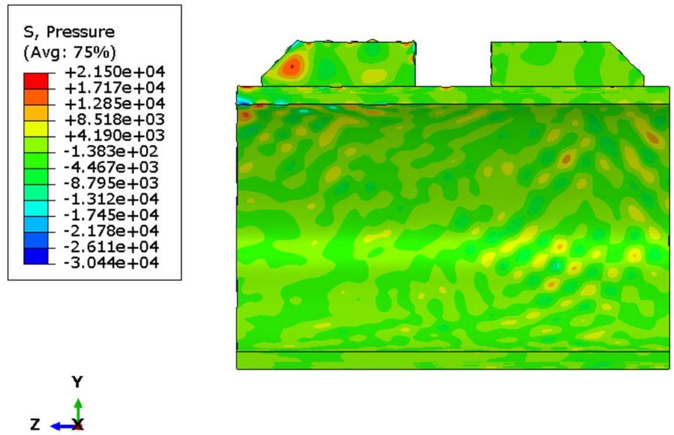

Figure 3) Pressure contour at increment 37334 and time 1.8667×10⁻4 s.

4. Results and Discussion

After completing the simulations, the results initially present the overall wave amplitude versus time over 200 microseconds for Model 1 (pure PMMA) at incident angles ranging from 40° to 75° in 5° increments, as shown in Figure 4. It should be noted that all signals have been normalized with respect to their peak values. Figures 5 and 6 display the corresponding signals for Model 2 (infinite element) and Model 3 (damping epoxy), respectively.

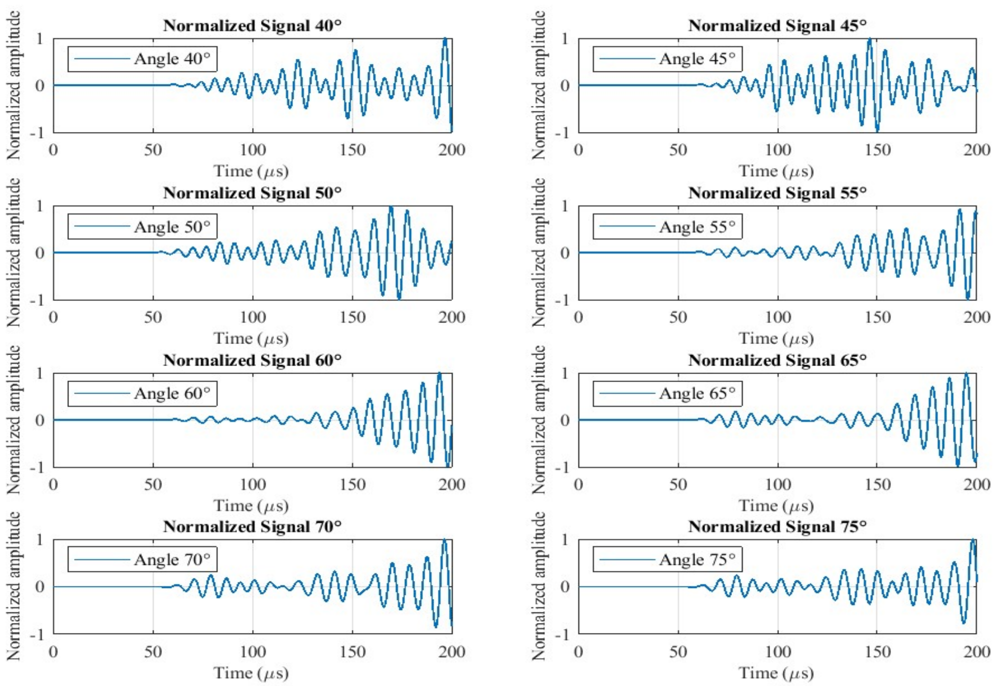

Figure 4) Time-Domain Amplitude of Model 1 (Pure PMMA Wedge)

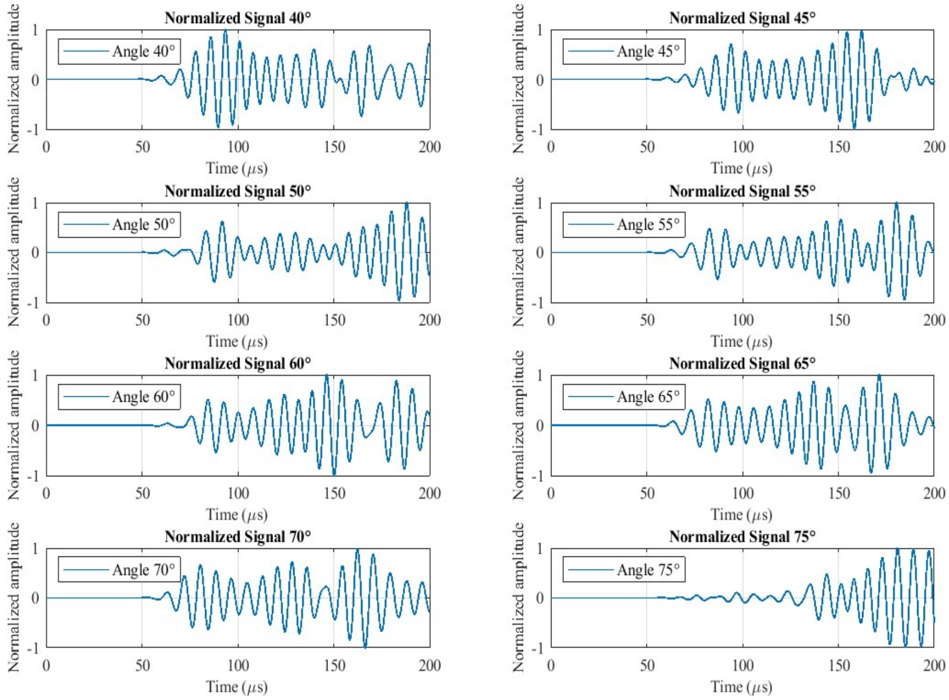

Figure 5) Time-Domain Amplitude of Model 2 (Infinite Element Wedge)

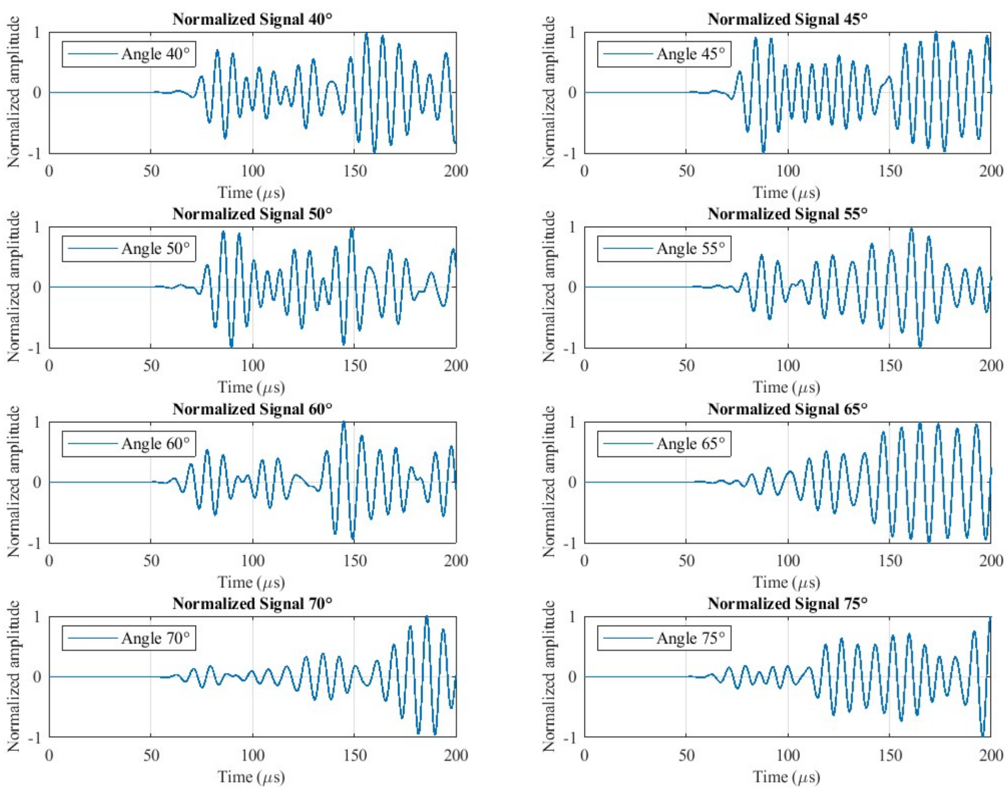

Figure 6) Normalized Time-Domain Amplitude of Model 3 (Damping Epoxy Wedge)

As illustrated in Figure 4, the largest peak in each signal occurs at different time intervals depending on the excitation angle. For the signal corresponding to the 45° incident angle, the first peak indicates that the mode generated at the initial portion of the signal is more clearly distinguishable compared to other angles. Additionally, the overall signal at this angle exhibits a narrower bandwidth, suggesting reduced wave dispersion.

In Figure 5 Model 2, the wave propagation signals differ markedly from those in Model 1, indicating a significant change in wave behavior due to the altered boundary conditions. Notably, Model 2 produces a greater number of peaks compared to the Model 1 setup. This increase in peaks can be attributed to Improved time–frequency resolution: With fewer spurious reflections to mask the signal, formerly overlapping modal components become separable in time and frequency domains. These observations align with prior research on the use of infinite or absorbing boundary conditions for wave simulations to isolate intrinsic wave behavior and reduce artificial reflections from truncated domains [25].

In Model 3 the initial peak amplitude is consistently higher across a broader range of incident angles compared to the first two configurations. This behaviour can be attributed to the viscoelastic damping layer incorporated into the wedge, which absorbs energy from waves reflecting off the wedge boundaries, thereby reducing interference from spurious internal reflections and allowing the primary guided wave to dominate the received signal. As reported in prior studies of wedge damping, such layers can improve measurement clarity by up to 10–30 dB through attenuation of interfering waves [26]. Similarly, research on wave propagation in viscoelastic coatings has shown that the presence of a damping layer significantly reduces unwanted mode coupling and reflection, thereby enhancing the clarity of the main transmitted mode [27].

To facilitate a more focused and meaningful comparison of the signals, the time window was restricted to the interval in which the first peak appears for all incident angles. Consequently, the signals were limited to the 50–110 µs range, enabling clearer evaluation and comparison. In Figure 4, the first peaks corresponding to different angles are presented. For clarity, only those angles exhibiting a significantly higher initial peak compared to others are shown to minimize signal overlap. It should be noted that all signals were time-shifted according to the difference in propagation path length resulting from the configuration of each wedge at its corresponding incidence angle. Specifically, the vertical distance between the wave source and the pipe surface was measured, and the arrival time of the wave at the pipe was calculated based on the longitudinal wave velocity in the PMMA wedge, obtained using the following relation [28]:

$$V_L = \sqrt{\frac{E(1-v)}{\rho(1+v)(1-2v)}} \tag{1}$$

where E is the Young's modulus, ν is Poisson's ratio, and ρ is the material density. Each signal was then shifted in time by this calculated travel time to ensure proper alignment of the wave arrivals for all incidence angles.

For each angle, the corresponding envelope is indicated by a dashed line, with the envelope peak highlighted. The maximum envelope amplitude denotes the angle at which the initial peak exhibits the highest magnitude, indicating the guided wave mode that is most distinct and readily separable from others. Figures 5 and 6 depict the signals and corresponding envelopes for the selected angles in Models 2 and 3, respectively.

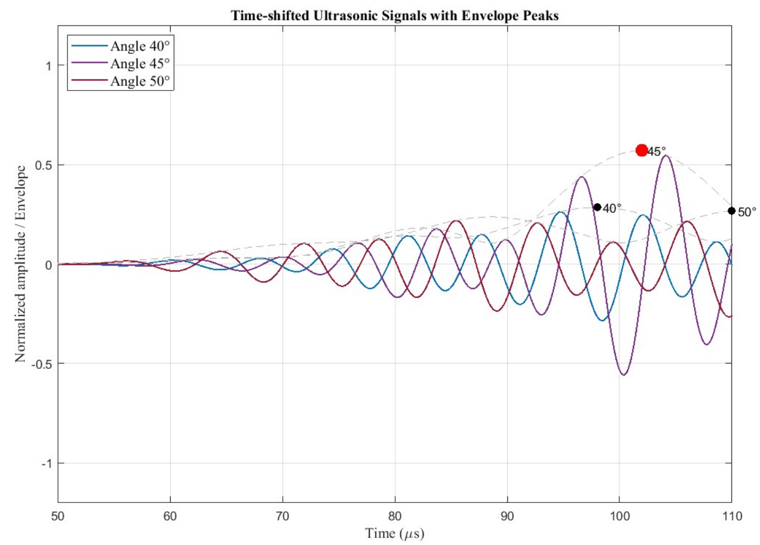

Figure 7) Normalized amplitude-time and the corresponding envelope within 50–110 µs for Model 1.

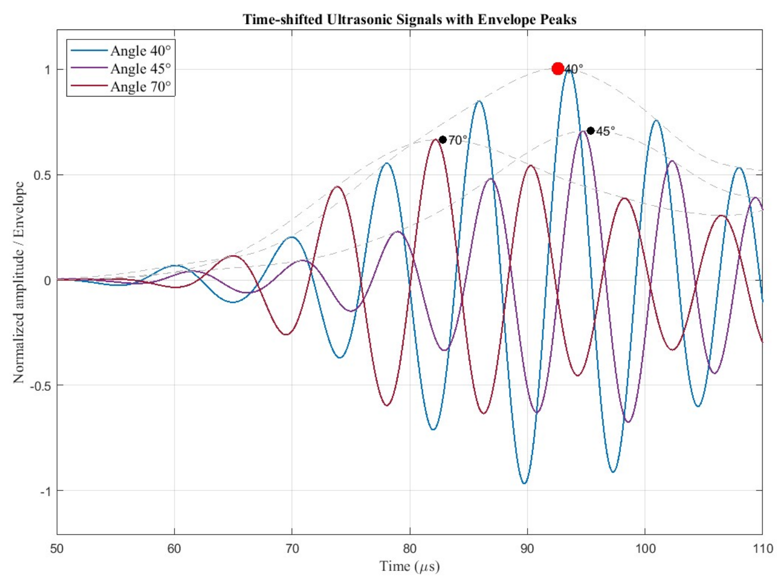

Figure 8) Normalized amplitude-time and the corresponding envelope within 50–110 µs for Model 2.

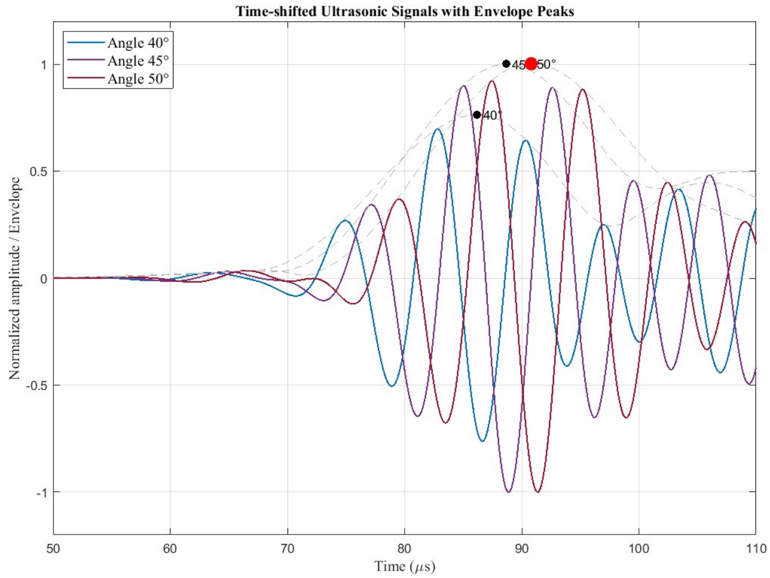

Figure 9) Normalized amplitude-time and the corresponding envelope within 50–110 μs for Model 3.

as shown in Figure 7, the signal corresponding to the 45° wedge exhibits the highest peak among all guided ultrasonic wave signals. The normalized peak amplitude of the 45° envelope is 0.57, which is 135% higher than the average of all peak values, indicating a significantly stronger response compared to the other excitation angles. In comparison, the 40° and 50° signals show lower peak amplitudes, demonstrating that the wave propagation is highly sensitive to the wedge angle, and the 45° configuration provides the optimal excitation for maximizing the signal response. It should be noted that the peaks and signal amplitudes at the other angles were smaller; therefore, they were omitted to avoid interference among signals and to facilitate clearer comparison and visualization.

in Figure 8 the signal at 40° exhibits the highest peak amplitude, measured as 1.004, which is approximately 71.4% higher than the mean peak amplitude of all other angles. This behavior implies that the 40° configuration corresponds to the optimal energy transmission or reflection condition for the examined setup. A pronounced increase in peak amplitudes is observed relative to the pure-PMMA condition. This difference is evident when comparing the maximum peaks between the two configurations. Moreover, the mean peak amplitude across all measured angles differs by 0.343 between the two conditions, indicating a systematic amplification of the response in the tested configuration. These results suggest that the modified configuration enhances the energy content of the transmitted/reflected signal.

In Figure 9, the signal at 50° exhibits the highest envelope peak amplitude, measured as 1.0023, which is approximately 78% greater than the mean peak amplitude of all other angles. It should also be noted that the peak at 45° attains an amplitude of 1.00021, which is extremely close to the maximum observed value. It is noteworthy that the average peak amplitudes in Models 2 and 3 are very similar, and the overall waveform shapes, as well as the initially excited modes, exhibit remarkable correspondence. This suggests that Models 2 and 3 demonstrate higher mutual consistency, indicating well-aligned underlying physical assumptions and boundary conditions. Furthermore, the close agreement in both amplitude and mode shape implies that these two simulation models more accurately capture the actual experimental behavior, providing greater reliability for subsequent comparative or predictive analyses.

The quantification of signal energy in ultrasonic guided-wave testing plays a critical role in evaluating wave propagation efficiency and mode excitation within structures. Signal energy offers a direct metric of the intensity of ultrasonic wave fields, which correlates with the detectability of specific vibration modes and the integrity of structural features [9]. Figure 10 and 11 illustrate the normalized signal energy for the infinite-element and damping-epoxy models, respectively, over the entire time window and within the 50–110 μs interval**.**

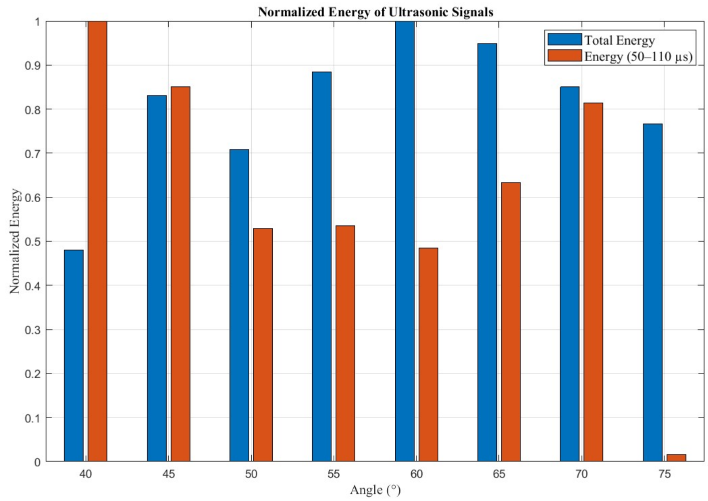

Figure 10) Normalized Total Energy vs. Energy in 50-110 μs for Infinite Element

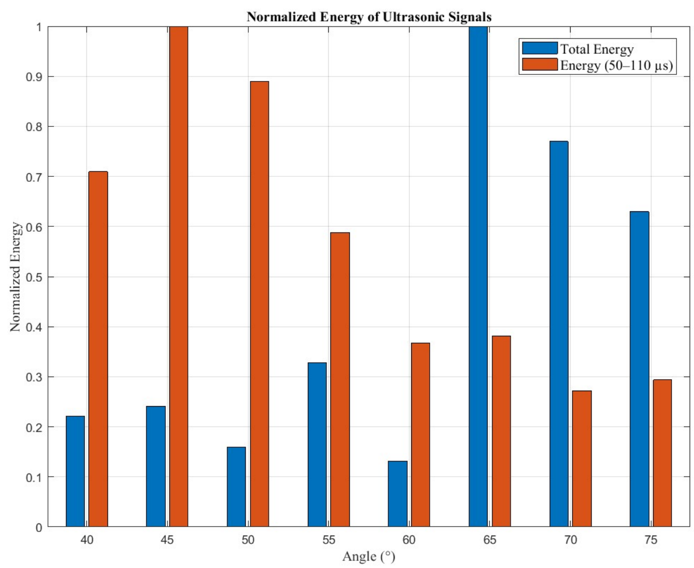

Figure 11) Normalized Total Energy vs. Energy in 50-110 μs for Damping Epoxy

In the case of the infinite-element model, the maximum total energy (over the full-time window) occurs at the 60° angle with a value of 33.76 (normalized units), whereas in the narrower time window of 50–110 μs (i.e., where the first peaks appear), the maximum energy shifts to 40° with a value of 8.18. For the damping-epoxy model, the highest total energy is observed at 65°, while in the 50–110 μs window, the highest energy corresponds to 45° with a value of 15.85.

5. Conclusion

In this study, a comprehensive comparison of ultrasonic guided-wave signals was conducted using three different simulation models, focusing on signal amplitude, peak characteristics, and energy distribution. The analysis revealed a pronounced sensitivity of wave propagation to the excitation angle and boundary conditions in three different models. In Model 1 (pure PMMA), the largest peaks occurred at different times depending on the incident angle, with the 45° configuration showing the clearest first mode and a narrower bandwidth, indicating reduced wave dispersion. Model 2 (infinite elements) exhibited an increased number of peaks compared to Model 1, due to improved time–frequency resolution and reduced spurious reflections, highlighting the importance of proper boundary conditions. In Model 3 (epoxy damping), the initial peak amplitudes were consistently higher across a wider range of angles, as the viscoelastic layer absorbed reflected energy. Time-shifted signals and envelope analyses were used to identify the angles corresponding to the highest initial peaks. In Models 2 (infinite elements) and 3 (epoxy damping), the peak amplitudes were generally higher than in Model 1. For Models 2 and 3, the average peak amplitudes and overall waveform shapes exhibited remarkable similarity, demonstrating high mutual consistency and well-aligned physical assumptions and boundary conditions. These findings suggest that both models more accurately replicate experimental behavior. Signal energy analysis further revealed critical insights. The total energy over the full-time window and the energy within the 50–110 μs interval—corresponding to the first excited modes—were computed and normalized for each angle. In the infinite-element model, the maximum total energy occurred at 60°, whereas the energy in the 50–110 μs window peaked at 40°. Similarly, for the damping-epoxy model, the highest total energy was observed at 65°, while the 50–110 μs window exhibited a maximum at 45°. Importantly, incident angles of 40°, 45°, and 50° consistently demonstrated superior performance across all models, showing both well-excited initial modes and higher peak amplitudes and energy within the targeted time interval.

These results indicate that the angle producing the highest overall energy does not necessarily correspond to the angle with the most clearly detectable modes. Overall, this study demonstrates that the optimal selection of incident angle to achieve both a strong first mode and high energy requires careful consideration of the initially excited modes. The findings emphasize the importance of integrating amplitude, peak, and energy analyses for accurate assessment of guided-wave propagation in experimental and simulation settings of composite pipes and materials, and provide a framework for optimizing measurement configurations in nondestructive evaluation.

REFERENCES

1. R. Rafiee, "On the mechanical performance of glass-fibre-reinforced thermosetting-resin pipes: A review," *Compos Struct*, vol. 143, pp. 151–164, 2016.
2. L. C. Hollaway, "A review of the present and future utilisation of FRP composites in the civil infrastructure with reference to their important in-service properties," *Constr Build Mater*, vol. 24, no. 12, pp. 2419–2445, 2010.
3. M. A. Karataş and H. Gökkaya, "A review on machinability of carbon fiber reinforced polymer (CFRP) and glass fiber reinforced polymer (GFRP) composite materials," *Defence Technology*, vol. 14, no. 4, pp. 318–326, 2018.
4. Carl Zweben, "Composite Materials," *Materials and Engineering Mechanics*, vol. Volume I., Feb. 2025.
5. R. Talreja and C. V. Singh, *Damage and failure of composite materials*. Cambridge University Press, 2012.

6. D. Ensminger and L. J. Bond, *Ultrasonics: fundamentals, technologies, and applications*. CRC press, 2024.
7. E. Mirmahdi, R. Khamedi, D. Afshari, and M. Khosravi, "Investigating the effects of defects and the effect of geometric anisotropy in stainless steel pipes: Phased array ultrasonic test, SH-wave," *Journal of Pipeline Science and Engineering*, vol. 3, no. 4, p. 100140, 2023.
8. J. L. Rose and P. Morrow, "An introduction to ultrasonic guided waves," in *4th middle east NDT conference and exhibition, Kingdom of Bahrain*, 2007.
9. S. C. Olisa, M. A. Khan, and A. Starr, "Review of current guided wave ultrasonic testing (GWUT) limitations and future directions," *Sensors*, vol. 21, no. 3, p. 811, 2021.
10. N. P. Yelve, M. Mitra, and P. M. Mujumdar, "Detection of delamination in composite laminates using Lamb wave based nonlinear method," *Compos Struct*, vol. 159, pp. 257–266, 2017.
11. E. Y. Maeva, I. Severina, and G. B. Chapman, "Ultrasonic analysis of the degree of cure and cohesive properties of the adhesive in a bond joint," *Research in Nondestructive Evaluation*, vol. 18, no. 2, pp. 121–138, 2007.
12. X. E. Gros, "Current and future trends in non-destructive testing of composite materials," in *Annales de Chimie Science des Matériaux*, Elsevier, 2000, pp. 539–544.
13. P. D. de Almeidaa, J. M. Alcoforado Rebello, G. R. Pereira, S. D. Soares, and R. Fernandez, "Ultrasonic inspection of adhesive joints of composite pipelines," in *AIP conference proceedings*, American Institute of Physics, 2014, pp. 1069–1076.
14. Z. Yang and Z. Wu, "Guided waves dispersion analysis in composite pipe using the safe method," in *European Workshop on Structural Health Monitoring*, Springer, 2020, pp. 727–738.
15. M. Gresil, A. Poohsai, and N. Chandarana, "Guided wave propagation and damage detection in composite pipes using piezoelectric sensors," *Procedia Eng*, vol. 188, pp. 148–155, 2017.
16. M. H. Soorgee and S. Jouzani, "Numerical Damage Detection in Composite Pipe Adhesive Joints Using Ultrasonic Guided Waves," *NDT Technology*, vol. 2, no. 6, pp. 72–81, 2020.
17. J. L. Rose, *Ultrasonic guided waves in solid media*. Cambridge university press, 2014.
18. Z. Wu *et al.*, "The decomposition of guided waves overlapped in the time–frequency domain in composite materials," *Applied Acoustics*, vol. 221, p. 110024, 2024.
19. A. Abuassal *et al.*, "A review of recent advances in unidirectional ultrasonic guided wave techniques for nondestructive testing and evaluation," *Sensors*, vol. 25, no. 4, p. 1050, 2025.
20. T. Feng, Z. Sharif Khodaei, and M. H. F. Aliabadi, "Influence of composite thickness on ultrasonic guided wave propagation for damage detection," *Sensors*, vol. 22, no. 20, p. 7799, 2022.
21. R. J. Kazys, J. Sestoke, and L. Mazeika, "Excitation and Reception of Higher-Order Guided Lamb Wave's A 1 and S 1 Modes in Plastic and Composite Materials," *Materials*, vol. 15, no. 20, p. 7249, 2022.
22. G. Veit and P. Belanger, "An ultrasonic guided wave excitation method at constant phase velocity using ultrasonic phased array probes," *Ultrasonics*, vol. 102, p. 106039, 2020.
23. H. Shi, L. Zhuang, X. Xu, Z. Yu, and L. Zhu, "An ultrasonic guided wave mode selection and excitation method in rail defect detection," *Applied Sciences*, vol. 9, no. 6, p. 1170, 2019.
24. J. Moll and C. P. Fritzen, "Advanced aspects of mode-selective excitation of ultrasonic guided waves," in *24th Conference on Noise and Vibration Engineering, 24th International Conference on Noise and Vibration Engineering*, 2010, pp. 969–984.
25. K. Hemalatha *et al.*, "Transverse wave propagation in functionally graded structures using finite elements with perfectly matched layers and infinite element coupling," *Mathematics*, vol. 13, no. 13, p. 2131, 2025.
26. O. Shapovalov, T. Heckel, M. Gaal, and S. Weiß, "External acoustical damping on a metallic

angle wedge in a high temperature resistant ultrasonic probe," *Acoust Aust*, vol. 50, no. 3, pp. 343–353, 2022.

27. X. Qi, *Ultrasonic guided waves for defect characterization in composite structures*. The Pennsylvania State University, 2011.

28. J. L. Rose, "A baseline and vision of ultrasonic guided wave inspection potential," *J Press Vessel Technol*, vol. 124, no. 3, pp. 273–282, 2002.